Available online at www.sciencedirect.com
ScienceDirect
Trans. Nonferrous Met. Soc. China 23(2013) 2029−2036
Transactions of Nonferrous Metals Society of China
www.tnmsc.cn

Phase transformation and damping behavior of lightweight porous TiNiCu alloys fabricated by powder metallurgy process

Hong-jie JIANG, Chang-bo KE, Shan-shan CAO, Xiao MA, Xin-ping ZHANG

School of Materials Science and Engineering, South China University of Technology, Guangzhou 510640, China

Received 28 January 2013; accepted 14 May 2013

Abstract: Porous TiNiCu ternary shape memory alloys (SMAs) were successfully fabricated by powder metallurgy method. The microstructure, martensitic transformation behavior, damping performance and mechanical properties of the fabricated alloys were intensively studied. It is found that the apparent density of alloys decreases with increasing the Cu content, the porous $Ti_{50}Ni_{40}Cu_{10}$ alloy exhibits wide endothermic and exothermic peaks arisen from the hysteresis of martensitic transformations, while the porous $Ti_{50}Ni_{30}Cu_{20}$ alloy shows much stronger and narrower endothermic and exothermic peaks owing to the B2-B19 transformation taking place easily. Moreover, the porous $Ti_{50}Ni_{40}Cu_{10}$ alloy shows a lower shape recovery rate than the porous $Ti_{50}Ni_{50}$ alloy, while the porous $Ti_{50}Ni_{30}Cu_{20}$ alloy behaves reversely. In addition, the damping capacity (or internal friction, IF) of the porous TiNiCu alloys increases with increasing the Cu content. The porous $Ti_{50}Ni_{30}Cu_{20}$ alloy has very high equivalent internal friction, with the maximum equivalent internal friction value five times higher than that of the porous $Ti_{50}Ni_{50}$ alloy.

Key words: porous TiNiCu alloys; powder metallurgy; martensitic transformation; damping behavior

1 Introduction

TiNi shape memory alloys (SMAs) have attracted significant interests due to their unique shape memory effect (SME), superelasticity and high damping performance [1−4]. These excellent physical and mechanical properties associated with the reversible martensitic transformation allow the commercial applications of TiNi SMAs in many fields, such as aerospace, biomedical and mechanical engineering [5,6].

Generally, the most commonly used TiNi and TiNi-based alloys represent the major family of shape memory alloys [7]. Adding a third alloying element, such as Hf, Zr, Nb, Cu and Fe into TiNi binary shape memory alloys can alter the transformation temperatures, transformation hysteresis and mechanical/ thermomechanical properties of the binary TiNi alloys. In general, selection of the third alloying elements is based on the application interests of TiNi-based alloys. It has been known that TiNi-based alloys possess high damping capacity [8,9], thus have high potential for engineering applications, such as vibration control and energy absorption devices. Among the TiNi-based alloys, TiNiCu ternary alloys have attracted great interests due to their high damping capacity, stabilized superelasticity characteristics against cyclic deformation and less composition sensitivity over the transformation temperatures in applications [10−12]. It has been demonstrated that adding Cu to TiNi alloy causes good stability of martensitic transformation temperature, narrow transformation hysteresis, good fatigue property and high damping property [12−15]. However, it is found that when Cu content is higher than 10% in mole fraction, the TiNiCu ternary alloys fabricated by the conventional melting and casting approaches exhibited the reduction in ductility [16], thus leading to certain limitations for industrial application of high Cu content and high damping TiNiCu alloy. So far, several studies have attempted to adopt the nonconventional techniques, including powder metallurgy (PM) [17], melt-spinning (MS) [18] and twin roll casting (TRC) [19]. The porous TiNiCu alloys prepared by the powder metallurgy technique possess lightweight and higher damping capacity over the porous TiNi alloy and thus show the great potential for commercial applications. The previous study employed powder metallurgy technique mainly focused on the sintering temperature, sintering time and

Foundation item: Projects (50871039, 51205135) supported by the National Natural Science Foundation of China; Project (S2011040001436) supported by the Guangdong Provincial Natural Science Foundation, China
Corresponding author: Xin-ping ZHANG; Tel: +86-20-22236396; E-mail: mexzhang@scut.edu.cn
DOI: 10.1016/S1003-6326(13)62692-8

porosity of the TiNiCu alloys. In contrast, relatively less attention has been paid to characterization of the mechanical behavior of porous TiNiCu ternary shape memory alloys, in particular the damping performance and mechanisms. In the present study, the powder metallurgy method was utilized to fabricate porous TiNiCu alloys; further, the microstructure, martensitic transformation behavior and damping performance of alloys as well as mechanical properties and shape recovery rate were characterized systematically.

2 Experimental

Titanium powder (50 μm, 99.9% purity), nickel powder (61 μm, 99.9% purity) and copper powder (75 μm, 99.7% purity) were weighed according to the designed compositions of $Ti_{50}Ni_{50}$, $Ti_{50}Ni_{40}Cu_{10}$ and $Ti_{50}Ni_{30}Cu_{20}$, and mixed for 24 h by an automatic motor-driven blender. Then, the sufficiently blended powders were cold compacted into short-bar green samples (16 mm×20 mm, diameter × height) and cuboid green samples (5 mm×7 mm×25 mm, thickness×width× length) respectively, with a compact stress of 200 MPa. The compacted green samples were heated to 1100 °C and held for 3 h in a quartz tube furnace under the protective flowing argon gas (99.99% purity) followed by water quenching. Finally, all samples were subjected to an aging treatment at 450 °C for 1 h followed by water quenching. In addition, a dense $Ti_{50}Ni_{30}Cu_{20}$ alloy was prepared by melting the compacted green samples in a non-consumable vacuum arc melting furnace (WK-1 model).

The porosity of the fabricated samples was measured by the relative density method through comparing with the dense one of the same composition, while the open porosity was determined by the drainage method. The pore features, microstructures and compositions of the fabricated samples were characterized by scanning electron microscopy (Quanta 200 and Nova NanoSEM, FEI) equipped with an energy-dispersive X-ray spectroscope (INCA X-act, Oxford). Phase constituents and martensitic transformation behavior of the alloys were analyzed by a Philips X’pert XRD and a differential scanning calorimeter (DSC Q200, TA), respectively. Mechanical properties of the TiNiCu alloys, including the compressive strength, superelasticity, residual deformation and shape recovery rate, were evaluated using a Shimadzu universal testing machine (AG-X 100 kN) with a strain rate of 3.33×10^{-3} s^{-1} at room temperature (25 °C). Test specimens used for mechanical tests were cylinder-shaped with geometry of 6 mm×12 mm (diameter×height). The internal friction behavior of the TiNiCu alloys with the test specimen geometry of 1.2 mm × 4 mm × 25 mm (thickness×width×length) was characterized using a dynamic mechanical analyzer (DMA Q800, TA) in the single-cantilever mode at a constant amplitude of 10 μm and 0.1 Hz vibration frequency in the temperature ranging from −120 °C to 120 °C with a constant heating/cooling rate of 5 °C/min.

3 Results and discussion

3.1 Microstructure and phase constituents of porous TiNiCu ternary alloys

The apparent density and pore characteristic parameters of the fabricated porous $Ti_{50}Ni_{50}$ and TiNiCu alloys are shown in Table 1. Clearly, the porosity, open porosity and average pore size of the porous TiNiCu alloys increase with increasing Cu content, while the apparent density of alloys decreases. It is worth noting that the porous $Ti_{50}Ni_{30}Cu_{20}$ alloy shows the lowest density of 4.0 g/cm^3, 38% lower than that of the dense $Ti_{50}Ni_{30}Cu_{20}$ alloy (6.50 g/cm^3). Figure 1 shows the second electron (SE) images of the porous $Ti_{50}Ni_{50}$, $Ti_{50}Ni_{40}Cu_{10}$ and $Ti_{50}Ni_{30}Cu_{20}$ alloys. It can be seen from Fig. 1(a), that there are many small and closed pores in the porous $Ti_{50}Ni_{50}$ alloy, which evenly distribute in the matrix of the alloy. On the other hand, in porous $Ti_{50}Ni_{40}Cu_{10}$ and $Ti_{50}Ni_{30}Cu_{20}$ alloys, there are many large pores shown in Figs. 1(b) and (c), and most of them connect each other, leading to high open porosity of 74% and 81% respectively as shown in Table 1. This is because that the diffusion rate of Cu atoms in Ti is higher than that of Ni atoms in Ti, which consequently leads to a significant increase of the volume of pores with increasing Cu content [17]. Moreover, as the melting point of Cu (1084 °C) is lower than the sintering temperature (1100 °C), under the sintering condition Cu particles can completely melt and penetrate into Ni and Ti powers, leading to increase in the reaction rate, reduction in the unreacted residual particles, connection of pores and densification of the matrix of the alloy. As a result, the addition of Cu in the TiNi based alloy tends to

Table 1 Apparent density and pore parameters of fabricated porous TiNi and TiNiCu alloys

Alloy	Apparent density/ (g·cm^{-3})	Porosity/ %	Open porosity/%	Mean pore size/μm
Porous $Ti_{50}Ni_{50}$	4.5	28	32	42
Porous $Ti_{50}Ni_{40}Cu_{10}$	4.2	35	74	105
Porous $Ti_{50}Ni_{30}Cu_{20}$	4.0	38	81	126
Dense $Ti_{50}Ni_{30}Cu_{20}$	6.5	–	–	–

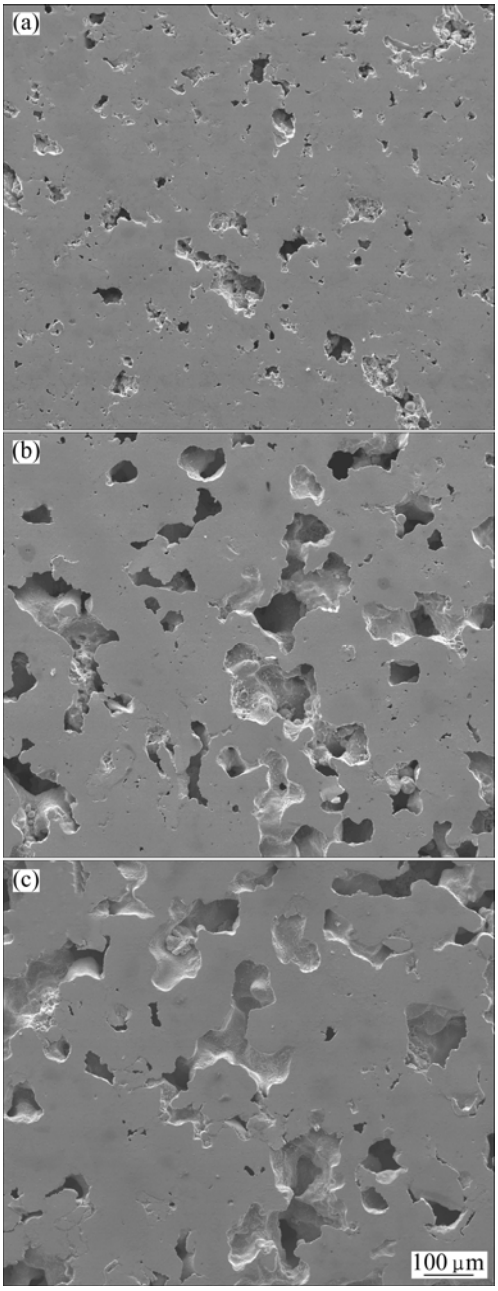

Fig. 1 Second electron (SE) images of porous alloys: (a) $Ti_{50}Ni_{50}$; (b) $Ti_{50}Ni_{40}Cu_{10}$; (c) $Ti_{50}Ni_{30}Cu_{20}$

increase the porosity and thus decrease the apparent density of the alloy.

The backscattered electron (BSE) images of the porous $Ti_{50}Ni_{40}Cu_{10}$ and $Ti_{50}Ni_{30}Cu_{20}$ alloys are shown in Fig. 2, and Table 2 shows the energy spectrum analysis results of precipitates in the alloys. In Fig. 2, a large

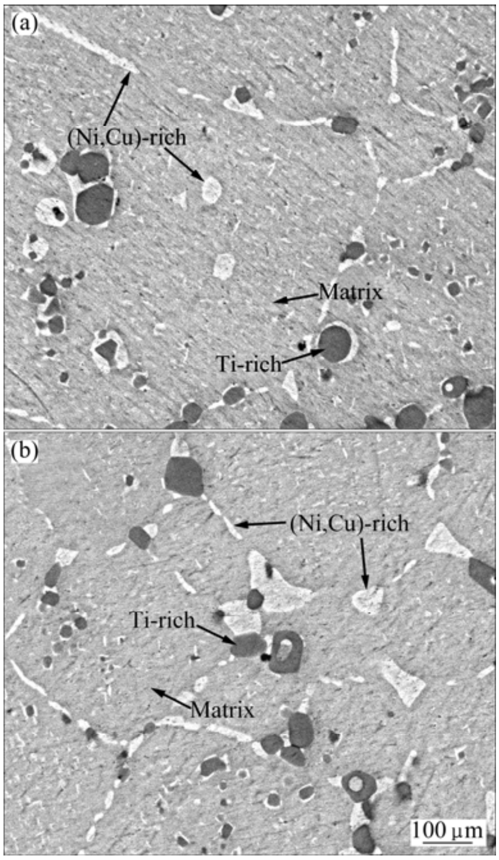

Fig. 2 Backscattered electron (BSE) images of porous alloys: (a) $Ti_{50}Ni_{40}Cu_{10}$; (b) $Ti_{50}Ni_{30}Cu_{20}$

number of dark Ti-rich particles and bright (Ni,Cu)-rich particles exist in the matrix of the alloy as confirmed by EDS analysis. It can be seen from Table 2 that the dark Ti-rich particles have low Cu content and the bright (Ni,Cu)-rich particles have high Cu content in both porous $Ti_{50}Ni_{40}Cu_{10}$ and $Ti_{50}Ni_{30}Cu_{20}$ alloys. With increasing Cu content, the relative concentration of Ni reduces and Ti content hardly changes in both the dark Ti-rich particles and bright (Ni,Cu)-rich particles. This is because that the solid solution of Cu only replaces Ni atom, as a result, the Ni content reduces and the Cu content increases in the dark Ti-rich and bright (Ni,Cu)-rich particles. Nevertheless, the mole ratio of "Ni+Cu" to Ti is unchanged in the TiNiCu alloys.

The XRD patterns of the porous $Ti_{50}Ni_{50}$, $Ti_{50}Ni_{40}Cu_{10}$ and $Ti_{50}Ni_{30}Cu_{20}$ alloys are shown in Fig. 3. The porous $Ti_{50}Ni_{50}$ alloy mainly consists of TiNi, Ti_2Ni and $TiNi_2$ phases, as shown in Fig. 3(a). The main phases

Table 2 Energy spectrum analysis results of precipitate particles in porous TiNiCu alloys

Alloy	Ti-rich particle			(Ni,Cu)-rich particle			Matrix		
	x(Ti)/%	x(Ni)/%	x(Cu)/%	x(Ti)/%	x(Ni)/%	x(Cu)/%	x(Ti)/%	x(Ni)/%	x(Cu)/%
$Ti_{50}Ni_{40}Cu_{10}$	64.32	29.52	6.16	37.72	45.82	16.46	41.49−43.51	48.64−50.14	6.35−9.47
$Ti_{50}Ni_{30}Cu_{20}$	64.82	22.08	13.10	38.34	24.69	36.97	49.56−50.09	31.52−32.31	17.59−18.92

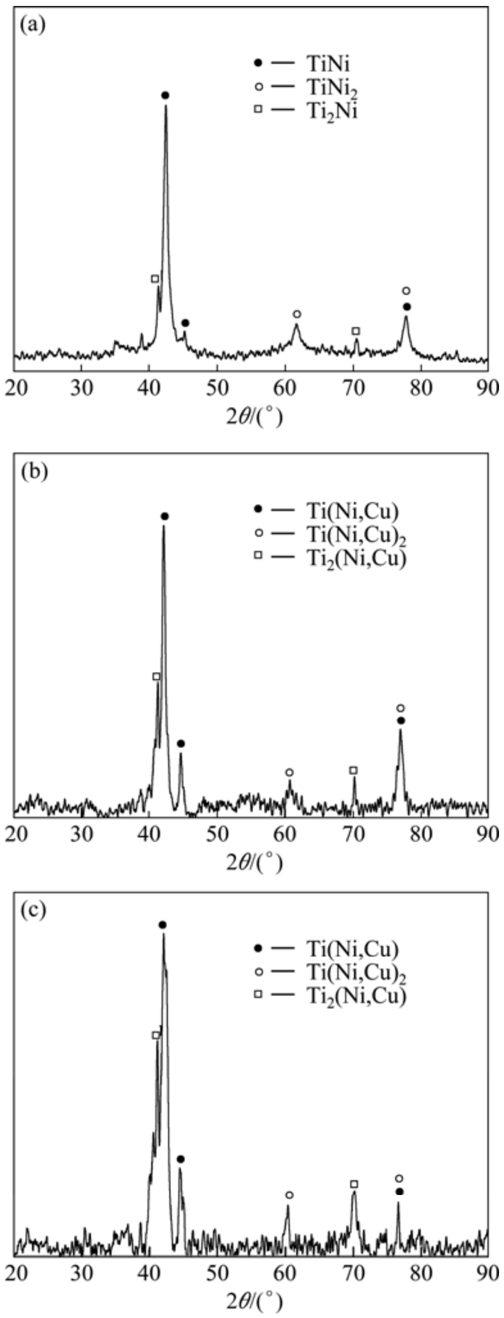

Fig. 3 XRD patterns of porous alloys: (a) $Ti_{50}Ni_{50}$; (b) $Ti_{50}Ni_{40}Cu_{10}$; (c) $Ti_{50}Ni_{30}Cu_{20}$

of the porous $Ti_{50}Ni_{40}Cu_{10}$ and $Ti_{50}Ni_{30}Cu_{20}$ alloys are Ti(Ni,Cu), Ti_2(Ni,Cu) and Ti(Ni, Cu)$_2$, as shown in Figs. 3(b) and (c), where the dark Ti-rich particles are Ti_2(Ni,Cu) and the bright Ni-rich particles are Ti(Ni,Cu)$_2$. Clearly, the microstructure and phase constituents of the $Ti_{50}Ni_{50}$ binary alloy have changed significantly after adding Cu element.

3.2 Phase transformation behavior of porous TiNiCu ternary alloys

Figure 4 shows DSC curves of the porous $Ti_{50}Ni_{50}$, $Ti_{50}Ni_{40}Cu_{10}$ and $Ti_{50}Ni_{30}Cu_{20}$ alloys. Table 3 gives the transformation temperatures of the alloys. During cooling, M_s, M_f and P_C represent the martensite transformation start temperature, martensite

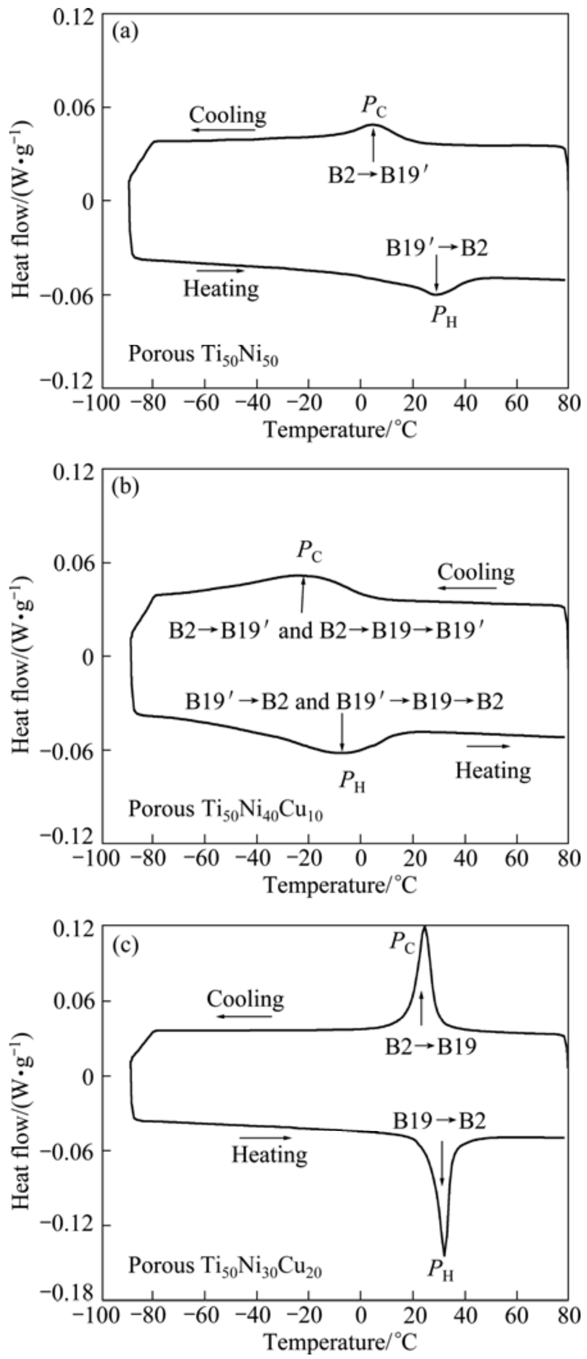

Fig. 4 DSC curves of porous alloys: (a) $Ti_{50}Ni_{50}$; (b) $Ti_{50}Ni_{40}Cu_{10}$; (c) $Ti_{50}Ni_{30}Cu_{20}$

Table 3 Transformation temperatures of fabricated porous TiNi and TiNiCu alloys

Alloy	M_s/°C	M_f/°C	A_s/°C	A_f/°C	P_C/°C	P_H/°C
$Ti_{50}Ni_{50}$	21	−17	−18	42	5	29
$Ti_{50}Ni_{40}Cu_{10}$	6	−59	−55	16	−24	−7
$Ti_{50}Ni_{30}Cu_{20}$	36	8	19	39	24	32

transformation finish temperature and transformation peak temperature, respectively. During heating, A_s, A_f and P_H represent the austenite transformation start temperature, austenite transformation finish temperature and transformation peak temperature, respectively. In Fig. 4(a), for porous $Ti_{50}Ni_{50}$ alloy only one phase transformation peak appears during heating and cooling, which corresponds to the B2→B19' and B19'→B2 phase transformation, respectively. In Fig. 4(b), two types of phase transformations take place in the porous $Ti_{50}Ni_{40}Cu_{10}$ alloy, which are B2-B19′ and B2-B19-B19′ during heating and cooling, respectively. In Fig. 4(c), only one phase transformation peak appears in the porous $Ti_{50}Ni_{30}Cu_{20}$ alloy during heating and cooling, which is corresponding to the one-step B2→B19 and B19→B2 phase transformation, respectively.

It can be seen from Fig. 4 and Table 3 that DSC curves of the porous $Ti_{50}Ni_{40}Cu_{10}$ alloy shows wider endothermic and exothermic peaks compared with DSC curves of the porous $Ti_{50}Ni_{50}$ alloy. However, in contrast, the DSC curves of the porous $Ti_{50}Ni_{30}Cu_{20}$ alloy shows much stronger and narrower endothermic and exothermic peaks. This can be understood by the Cu-content dependent transformation path in the Ti−Ni−Cu alloys. It has been reported that the addition of Cu contributes to the phonon softening of the Ti−Ni−Cu alloys and thus alters the intrinsic stability of the possible transformation products, which finally leads to a two-stage transformation of B2-B19-B19′, or even ends it at the stage of B2-B19 with a relative high Cu content [7]. Furthermore, the internal strain introduced by coherent $Ti(Ni,Cu)_2$ precipitates in the matrix of Ti−Ni−Cu alloys also promotes the B2-B19 transformation of the Ti−Ni−Cu alloys [20]. In the present study, as for the porous $Ti_{50}Ni_{40}Cu_{10}$ alloy, the Cu content in the matrix of the alloy is between 6.35% and 9.47% (see Table 2); the variation of Ni concentration in different micro-regions not only induces the change of martensitic transformation modes characterized by B2-B19′ and B2-B19-B19′ transition in the matrix of the alloy [13], but also brings about the discontinuous (or asynchronous) martensitic transformation, leading to the temperature hysteresis of martensitic transformation in the matrix of the alloy. So, the alloy shows broad transformation temperature ranges and weak transformation peaks during heating and cooling. On the other hand, for the porous $Ti_{50}Ni_{30}Cu_{20}$ alloy, only one-step B2-B19 transformation takes place in the matrix of the alloy with Cu concentration higher than 17.59% (see Table 2) [13]. Since the twin boundaries in B19 are much easier to move than those in B19′ [21], the martensitic transformation proceeds more easily and faster in the matrix of the alloy. Therefore, the porous $Ti_{50}Ni_{30}Cu_{20}$ alloy shows narrow transformation temperature ranges and sharp transformation peaks.

3.3 Mechanical properties of porous TiNiCu ternary alloys

Figure 5 shows the stress—strain curves of porous $Ti_{50}Ni_{50}$, $Ti_{50}Ni_{40}Cu_{10}$ and $Ti_{50}Ni_{30}Cu_{20}$ alloys subjected to five compressive cycles (C1−C5) at a strain level of 4%. The maximum compressive strengths of porous $Ti_{50}Ni_{50}$, $Ti_{50}Ni_{40}Cu_{10}$ and $Ti_{50}Ni_{30}Cu_{20}$ alloys are 285, 231 and 182 MPa, respectively. Clearly, the compressive strength of the porous TiNiCu alloys decreases with increasing Cu content. This is because the TiNiCu ternary alloy has $Ti(Ni, Cu)_2$ phase in the matrix, whose Vickers microhardness decreases with increasing Cu content [22]. In addition, the pinning effect of these $Ti(Ni, Cu)_2$ phases on motion of dislocations and interfaces as well as deformation of the TiNiCu alloy matrix becomes weaker with increasing Cu content, resulting in lower compressive strength of the alloy. Furthermore, the porosity ratio and pore size of porous TiNiCu alloys increase with increasing Cu content (as shown in Table 1), leading to the decrease of the volume fraction of the matrix in the porous TiNiCu alloys and finally resulting in the decreasing compressive strength of the porous TiNiCu alloys. Also, it can be seen from Fig. 5 that after the first compression loading cycle, which actually functions as training, the residual strains for the porous $Ti_{50}Ni_{50}$, $Ti_{50}Ni_{40}Cu_{10}$ and $Ti_{50}Ni_{30}Cu_{20}$ alloys are 1.0%, 1.3% and 2.0%, respectively, which increases with increasing the Cu content. Figure 5 also demonstrates that after the first compression loading cycle, a stable linear superelasticity has been attained in the porous TiNiCu alloys.

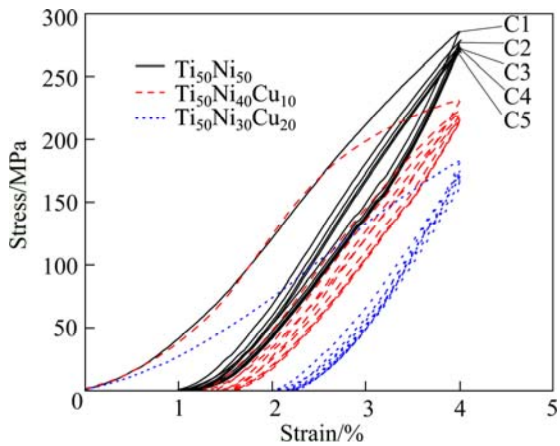

Fig. 5 Strain—stress curves of porous $Ti_{50}Ni_{50}$, $Ti_{50}Ni_{40}Cu_{10}$ and $Ti_{50}Ni_{30}Cu_{20}$ alloys under strain level of 4%

At a strain lever of 4%, the shape recovery rates of the porous $Ti_{50}Ni_{50}$, $Ti_{50}Ni_{40}Cu_{10}$ and $Ti_{50}Ni_{30}Cu_{20}$ alloys are 57.1%, 46.7% and 61.9%, respectively. Clearly, the porous $Ti_{50}Ni_{30}Cu_{20}$ alloy possesses the highest shape recovery rate and $Ti_{50}Ni_{40}Cu_{10}$ stays the lowest. This interesting scenario can be explained as follows. As mentioned above, the B2-B19 martensitic transformation takes place dominantly in the $Ti_{50}Ni_{30}Cu_{20}$ alloy, while the multi-step transformation of B2-B19′ and B2-B19-B19′ occurs in the $Ti_{50}Ni_{40}Cu_{10}$ alloy. It is the discontinuous (or asynchronous) martensitic transformation occurring in the alloy that leads to the discontinuity of shape recovery behavior of the alloy. The twin boundaries in B19 phase move much easier than those in B19′ phase, making the B2-B19 martensitic transformation take place more easily and faster in the matrix of the alloy, and consequently resulting in a higher shape recovery rate of the porous $Ti_{50}Ni_{30}Cu_{20}$ alloy. Moreover, the relatively soft $Ti(Ni, Cu)_2$ phase particles, whose microhardness decreases with Cu content [22], can weaken the pinning effect of $Ti(Ni, Cu)_2$ particles on movement of dislocations and sliding of interfaces in the matrix of the $Ti_{50}Ni_{30}Cu_{20}$ alloy. Consequently, the martensitic transformation proceeds more easily in the matrix of the alloy and the recovery resistance of the alloy decreases, and finally the shape recovery rate of the porous $Ti_{50}Ni_{30}Cu_{20}$ alloy can be further increased.

3.4 Damping behavior of porous TiNiCu ternary alloys

Figure 6 shows the results of internal friction (IF) versus temperature for the porous $Ti_{50}Ni_{50}$, $Ti_{50}Ni_{40}Cu_{10}$ and $Ti_{50}Ni_{30}Cu_{20}$ alloys, where the internal friction tests were performed using a vibration frequency of 0.1 Hz and amplitude of 10 μm. Apparently, the maximum values of internal friction peaks, denoted by P_α, of the porous $Ti_{50}Ni_{50}$, $Ti_{50}Ni_{40}Cu_{10}$ and $Ti_{50}Ni_{30}Cu_{20}$ alloys appear at −76.83 °C, −73.89 °C and 7.84 °C, and correspondingly the IF values of P_α are 0.035, 0.120 and 0.160, respectively. Further, during heating, the maximum values of internal friction peaks, denoted by P_β, of the porous $Ti_{50}Ni_{50}$, $Ti_{50}Ni_{40}Cu_{10}$ and $Ti_{50}Ni_{30}Cu_{20}$ alloys appear at 31.76 °C, −26.13 °C and 47.78 °C, corresponding to the IF values of 0.032, 0.113 and 0.169, respectively. Clearly, the internal friction peak value of porous TiNiCu alloys increases with increasing Cu content. Noticeably, the maximum IF value of the porous $Ti_{50}Ni_{30}Cu_{20}$ alloy is 357 % higher than that of the porous $Ti_{50}Ni_{50}$ alloy. However, the porous $Ti_{50}Ni_{40}Cu_{10}$ alloy shows the lower IF level and the broadest IF temperature range among three types of alloys.

In our previous studies [23,24], a parameter named equivalent internal friction (Q_{eq}^{-1}) was proposed to characterize the effective internal friction of the materials with different porosities in a normalized way, which is expressed by the following equation $Q_{eq}^{-1} = Q^{-1}/(1-P)$, where Q^{-1} is the measured internal friction, and P is

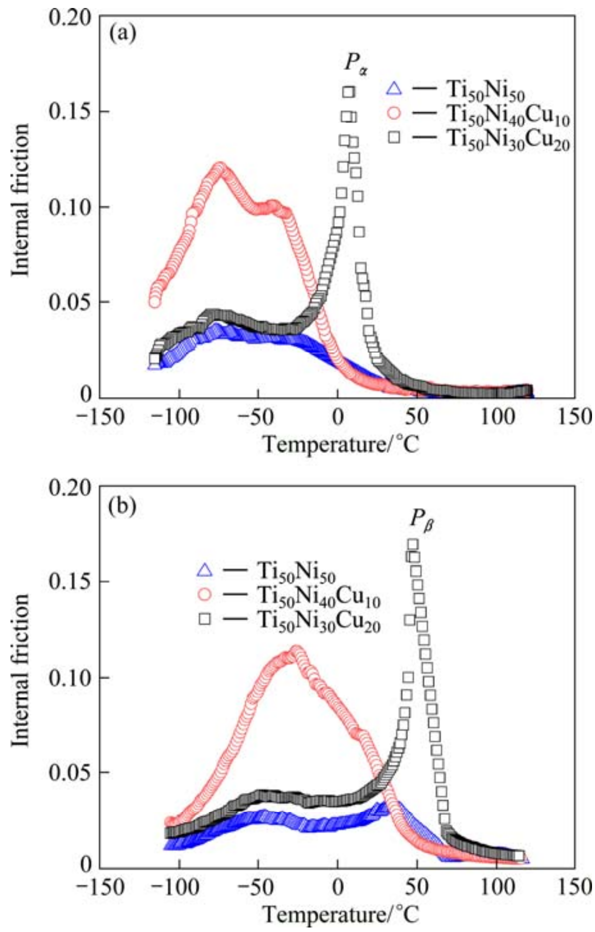

Fig. 6 Curves of internal friction vs temperature for porous $Ti_{50}Ni_{50}$, $Ti_{50}Ni_{40}Cu_{10}$ and $Ti_{50}Ni_{30}Cu_{20}$ alloys measured at 0.1 Hz on cooling (a) and on heating (b)

the porosity. Figure 7 shows the equivalent internal friction curves of the porous $Ti_{50}Ni_{50}$, $Ti_{50}Ni_{40}Cu_{10}$ and $Ti_{50}Ni_{30}Cu_{20}$ alloys under 10 μm amplitude and 0.1 Hz vibration frequency. The maximum values of Q_{eq}^{-1} for three alloys are 0.049, 0.185 and 0.273, respectively, in which the porous $Ti_{50}Ni_{30}Cu_{20}$ alloy has the highest equivalent internal friction, five times higher than that of the porous $Ti_{50}Ni_{50}$ alloy.

The internal friction (or damping) mechanisms in the porous TiNiCu alloys are intrinsically related to the martensitic transformation and interface behavior. During the thermal (heating and cooling) and mechanical (vibration) loading process, in the porous $Ti_{50}Ni_{30}Cu_{20}$ alloy the B2→B19 transformation exhibits a dramatic lattice-softening phenomenon and twin boundaries in B19 phase move much easier than those in B19′ phase (which was also reflected in the DSC curve with sharp and strong transformation peaks), resulting in a higher damping capacity. Furthermore, it is known that the movement of interfaces and twin boundaries can be impeded by the precipitate particles [25]. The relatively soft $Ti(Ni,Cu)_2$ particles formed in the TiNiCu alloy with

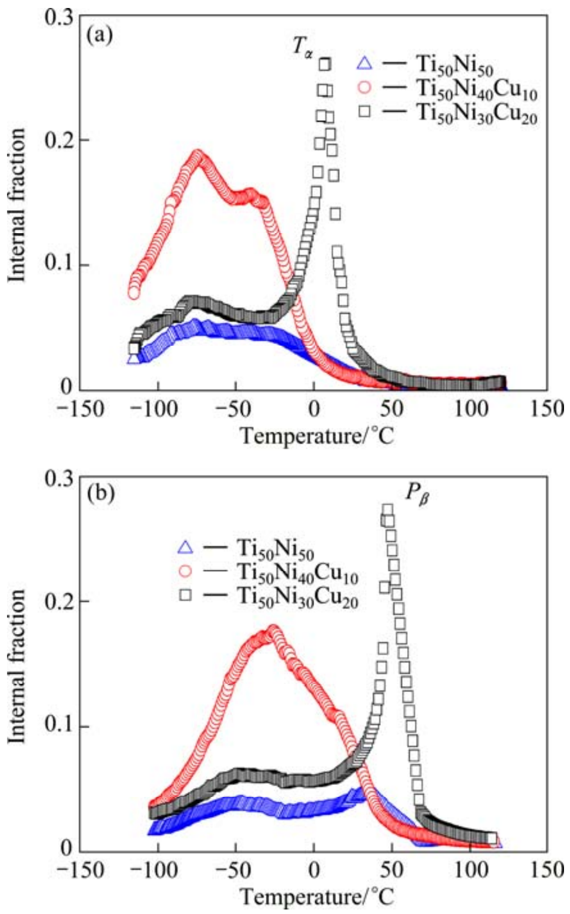

Fig. 7 Curves of equivalent internal friction vs temperature for porous $Ti_{50}Ni_{50}$, $Ti_{50}Ni_{40}Cu_{10}$ and $Ti_{50}Ni_{30}Cu_{20}$ alloys measured at 0.1 Hz on cooling (a) and on heating (b)

a higher Cu content would weaken the pinning effect of $Ti(Ni,Cu)_2$ particles on the motion of interfaces and dislocations in the alloy matrix. This in turn would promote the conversion of external vibration energy into internal energy, consequently leading to a high damping capacity of the alloy. As a result of the above factors, the porous $Ti_{50}Ni_{30}Cu_{20}$ alloy exhibits much higher maximum equivalent internal friction value than the porous $Ti_{50}Ni_{50}$ alloy. In addition, for the porous $Ti_{50}Ni_{40}Cu_{10}$ alloy, both the single-step B2-B19′ and multi-step B2-B19-B19′ transformations (as shown in Fig. 4) take place in the matrix of the alloy at different temperatures, which give rise to the discontinuous character of martensitic transformation. As a result, the porous $Ti_{50}Ni_{40}Cu_{10}$ alloy shows a wide IF temperature range.

4 Conclusions

1) Porous TiNiCu ternary shape memory alloys were successfully fabricated by powder metallurgy process. The apparent density of the porous TiNiCu ternary alloy decreases with increasing Cu content and is obviously lower than that of the dense TiNiCu ternary alloy.

2) The porous $Ti_{50}Ni_{40}Cu_{10}$ alloy shows wide endothermic and exothermic peaks arisen from the hysteresis of both B2-B19′ and B2-B19-B19′ transformations. The porous $Ti_{50}Ni_{30}Cu_{20}$ alloy exhibits much stronger and narrower endothermic and exothermic peaks owing to occurrence of the single-step B2-B19 transformation easy.

3) The porous $Ti_{50}Ni_{30}Cu_{20}$ alloy exhibits a higher shape recovery rate than the porous $Ti_{50}Ni_{50}$ alloy, while the porous $Ti_{50}Ni_{40}Cu_{10}$ alloy shows a lower shape recovery rate than the porous $Ti_{50}Ni_{50}$ alloy.

4) The internal friction of porous TiNiCu ternary alloys increases with increasing Cu content. The porous $Ti_{50}Ni_{30}Cu_{20}$ alloy has very high equivalent internal friction, with the maximum equivalent internal friction value, five times higher than that of the porous $Ti_{50}Ni_{50}$ alloy.

References

[1] LIU Y, van HUMBEECK J, STALMANS R, DELAEY L. Some aspects of the properties of NiTi shape memory alloy [J]. Journal of Alloys and Compounds, 1997, 247(1): 115−121.

[2] OTSUKA K, WAYMAN C M. Shape memory materials [M]. Cambridge: Cambridge University Press, 1998: 49−96.

[3] JIANG Shu-yong, ZHANG Yan-qiu. Microstructure evolution and deformation behavior of as-cast NiTi shape memory alloy under compression [J]. Transactions of Nonferrous Metals Society of China, 2012, 22: 90−96.

[4] JIANG Shu-yong, ZHANG Yan-qiu, ZHAO Ya-nan. Dynamic recovery and dynamic recrystallization of NiTi shape memory alloy under hot compression deformation [J]. Transactions of Nonferrous Metals Society of China, 2013, 23(1): 140−147.

[5] DOLCE M, CARDONE D. Mechanical behaviour of shape memory alloys for seismic applications [J]. International Journal of Mechanical Sciences, 2001, 43(11): 2657−2677.

[6] SAADAT S, SALICHS J, NOORI M, HOU Z, DAVOODI H, BAR-ON I, SUZUKI Y, MASUDA A. An overview of vibration and seismic applications of NiTi shape memory alloy [J]. Smart Materials and Structures, 2002, 11(2): 218−229.

[7] OTSUKA K. REN X. Physical metallurgy of TiNi-based shape memory alloys [J]. Progress in Materials Science, 2005, 50(5): 511−678.

[8] LIN H C, WU S K, CHANG Y C. Damping characteristics of $Ti_{50}Ni_{49.5}Fe_{0.5}$ and $Ti_{50}Ni_{40}Cu_{10}$ ternary shape memory alloys [J]. Metallurgical and Materials Transactions A, 1995, 26(4): 851−858.

[9] CAI W, LU X L, ZHAO L C. Damping behavior of TiNi-based shape memory alloys [J]. Materials Science and Engineering A, 2005, 394(1): 78−82.

[10] BISCARINI A, COLUZZI B, MAZZOLAI G, TUISSI A, MAZZOLAI F M. Extraordinary high damping of hydrogen-doped NiTi and NiTiCu shape memory alloys [J]. Journal of Alloys and Compounds, 2003, 355(1): 52−57.

[11] GIL F J, PLANELL J A. Effect of copper addition on the superelastic behavior of Ni−Ti shape memory alloys for orthodontic applications [J]. Journal of Biomedical Materials Research, 1999, 48(5): 682−688.

[12] YOSHIDA I, MONMA D, IINO K, OTSUKA K, ASAIC M, TSUZUKI H. Damping properties of $Ti_{50}Ni_{50-x}Cu_x$ alloys utilizing

martensitic transformation [J]. Journal of Alloys and Compounds, 2003, 355(1): 79−84.

[13] NAM T H, SABURI T, SHIMIZU K. Cu-content dependence of shape memory characteristics in Ti−Ni−Cu alloys [J]. Materials Transactions, 1990, 31(11): 959−967.

[14] GROSSMANN C, FRENZEL J, SAMPATH V, DEMPATH T, DEPKA T, EGGELER G. Elementary transformation and deformation processes and the cyclic stability of NiTi and NiTiCu shape memory spring actuators [J]. Metallurgical and Materials Transactions A, 2009, 40(11): 2530−2544.

[15] NESPOIL A, VILLA E, BESSEGHINI S. Characterization of the martensitic transformation in $Ni_{50-x}Ti_{50}Cu_x$ alloys through pure thermal measurements [J]. Journal of Alloys and Compounds, 2011, 509(3): 644−647.

[16] LIU Y. Mechanical and thermomechanical properties of a $Ti_{50}Ni_{25}Cu_{25}$ melt spun ribbon [J]. Materials Science and Engineering A, 2003, 354(1): 286−291.

[17] GORYCZKA T, van HUMBEECK J. NiTiCu shape memory alloy produced by powder technology [J]. Journal of Alloys and Compounds, 2008, 456(1): 194−200.

[18] SANTAMARTA R, CESARI E, PONS J, GORYCZKA T. Shape memory properties of Ni−Ti based melt-spun ribbons [J]. Metallurgical and Materials Transactions A, 2004, 35(3): 761−770.

[19] DALLE F, DESPERT G, VREMAUT P, PORTIER R, DEZELLUS A, PLAINDOUX P, OCHIN P. $Ni_{49.8}Ti_{42.2}Hf_8$ shape memory alloy strips production by the twin roll casting technique [J]. Materials Science and Engineering A, 2003, 346(1): 320−327.

[20] FUKUDA T, KITAYAMA M, KAKESITA T, SABURI T. Martensitic transformation behavior of a shape memory Ti−40.5Ni−10Cu alloy affected by the $C11_b$-type precipitates [J]. Materials Transactions, 1996, 37(10): 1540−1546.

[21] YOSHIDA I, MONMA D, IINO K, ONO T, OTSUKA K, ASAI M. Internal friction of Ti−Ni−Cu ternary shape memory alloys [J]. Materials Science and Engineering A, 2004, 370(1): 444−448.

[22] FUKUDA T, KAHESITA T, SABURI T. Copper content dependence of the lattice parameters of $Ti(NiCu)_2$ [J]. Materials Transactions, 2000, 41(7): 837−840.

[23] ZHANG Yu-peng, ZHANG Xin-ping. Internal friction behaviors of porous NiTi alloys with variable porosities [J]. The Chinese Journal of Nonferrous Metals, 2009, 19(10): 1872−1879. (in Chinese)

[24] JIANG Hong-jie, KE Chang-bo, CAO Shan-shan, MA Xiao, ZHANG Xin-ping. Preparation of nano-sized SiC reinforced NiTi shape memory composites and their mechanical properties and damping behavior [J]. Acta Metallurgica Sinica, 2011, 47(9): 1105−1111. (in Chinese)

[25] MALLIK U S, SAMPATH V. Effect of composition and ageing on damping characteristics of Cu−Al−Mn shape memory alloys [J]. Materials Science and Engineering A, 2008, 478(1): 48−55.

粉末冶金法制备轻质多孔 TiNiCu 形状记忆合金的相变和阻尼行为

江鸿杰，柯常波，曹姗姗，马 骁，张新平

华南理工大学 材料科学与工程学院， 广州 510640

摘 要：利用梯级粉末烧结法成功制备出轻质高阻尼的多孔 TiNiCu 形状记忆合金，并对其组织、相变行为、阻尼性能以及力学性能进行深入研究。研究发现，所制备的多孔 TiNiCu 合金的表观密度随着 Cu 含量的增加而降低；在降温和升温过程中，由于多孔 $Ti_{50}Ni_{40}Cu_{10}$ 合金基体中相变的滞后和叠加而使其相变温度区间宽化，相变峰弱化；而多孔 $Ti_{50}Ni_{30}Cu_{20}$ 合金基体中发生 B2-B19 相变而使其具有窄的相变温度区间以及较高的相变峰；多孔 $Ti_{50}Ni_{40}Cu_{10}$ 合金的形状回复率低于多孔 $Ti_{50}Ni_{50}$ 合金的，而多孔 $Ti_{50}Ni_{30}Cu_{20}$ 合金的形状回复率则高于多孔 $Ti_{50}Ni_{50}$ 合金的。研究还表明，多孔 TiNiCu 合金的内耗值随着 Cu 含量的增加而增大，其中多孔 $Ti_{50}Ni_{30}Cu_{20}$ 合金的一个显著特性是具有很高的等效内耗，其最大等效内耗值是多孔 $Ti_{50}Ni_{50}$ 合金的 5 倍。

关键词：多孔 TiNiCu 合金；粉末冶金；马氏体相变；阻尼行为

(Edited by Hua YANG)